Published in final edited form as:
Bioconjug Chem. 2006 ; 17(3): 662–669. doi:10.1021/bc050345c.

Near-Infrared Fluorescent Deoxyglucose Analog for Tumor Optical Imaging in Cell Culture and in Living Mice

Zhen Cheng[†], **Jelena Levi**[†], **Zhengming Xiong**[†,‡], **Olivier Gheysens**[†], **Shay Keren**[†], **Xiaoyuan Chen**[†], and **Sanjiv Sam Gambhir**[†,*]

Molecular Imaging Program at Stanford (MIPS), Departments of Radiology and Bioengineering, Bio-X Program, Stanford University, California, California, 94305-5344

Department of Pediatrics, Tongji Medical College, Huazhong University of Science and Technology & Tongji Hospital, Wuhan, China, 430030

Abstract

2-deoxy-2-[^{18}F]fluoro-D-glucose ([^{18}F]FDG) has extensively been used for clinical diagnosis, staging and therapy monitoring of cancer and other diseases. Non-radioactive glucose analogs enabling the screening of the glucose metabolic rate of tumors are of particular interest for anticancer drug development. A non-radioactive fluorescent deoxyglucose analog may have many applications for both imaging of tumors and monitoring therapeutic efficacy of drugs in living animals and may eventually translate to clinical applications. We found that a fluorescent 2-deoxyglucose analog, 2-[*N*-(7-nitrobenz-2-oxa-1,3-diazol-4-yl)amino]-2-deoxy-D-glucose (2-NBDG) can be delivered in several tumor cells via the glucose transporters (GLUTs). We therefore conjugated D-glucosamine with a near-infrared (NIR) fluorphor Cy5.5 and tested the feasibility of Cy5.5-D-glucosamine conjugate (Cy5.5-2DG) for NIR fluorescence imaging of tumors in a pre-clinical xenograft animal model. Cy5.5-2DG was prepared by conjugating Cy5.5 monofunctional N-hydroxysuccinimide ester (Cy5.5-NHS) and D-glucosamine followed by high-performance liquid chromatography purification. The accumulation of Cy5.5-2DG and Cy5.5-NHS in different tumor cell lines at 37 °C and 4 °C were imaged using a fluorescence microscope. Tumor targeting and retention of Cy5.5-2DG and Cy5.5-NHS in a subcutaneous U87MG glioma and A375M melanoma tumor model were evaluated and quantified by a Xenogen IVIS 200 optical cooled charged-coupled device system. Fluorescence microscopy imaging shows that Cy5.5-2DG and Cy5.5-NHS are taken up and trapped by a variety of tumor cell lines at 37 °C incubation, while they exhibit marginal uptake at 4 °C. The tumor cell uptake of Cy5.5-2DG can not be blocked by the 50 mM D-glucose, suggesting that Cy5.5-2DG may not be delivered in tumor cells by GLUTs. U87MG and A375M tumor localization were clearly visualized in living mice with both NIR fluorescent probes. Tumor/muscle contrast was clearly visible as early as 30 min post-injection, and the highest U87MG tumor/muscle ratio of 2.81 ± 0.10, 3.34 ± 0.23 were achieved 24 hours post-injection for Cy5.5-2DG and Cy5.5-NHS, respectively. While as a comparison, the micro-positron emission tomography imaging study shows that [^{18}F]FDG preferentially localize to the U87MG tumor, with resulting tumor/muscle ratios ranging from 3.89 to 4.08 after 30 min to 2 h post-administration of the probe. In conclusion, the NIR fluorescent glucose analog, Cy5.5-2DG and Cy5.5-NHS both demonstrate tumor targeting abilities in cell culture and in living mice. More studies are warranted to further explore their application for optical tumor imaging. In order to develop NIR glucose analog with ability to targeting GLUTs/hexokinase, it is highly important to select NIR dyes with reasonable molecular size.

*Author to whom correspondence should be addressed: Sanjiv Sam Gambhir M.D., Ph.D., Molecular Imaging Program at Stanford, Departments of Radiology and Bioengineering, Bio-X Program, 318 Campus Dr., Clark Center, E-150, Stanford University, Stanford, CA 94305, 650-725-2309 (V), 650-724-4948(Fax), sgambhir@stanford.edu.

Keywords

Near-infrared fluorescence; Glucose; Cy5.5; FDG; molecular imaging

INTRODUCTION

Positron emission tomography (PET) has become a generally accepted technique for pre-clinical and clinical noninvasive imaging of disease, especially cancer (1–3). Tracers enabling the targeting of specific cellular and molecular processes are major driving forces that have contributed to the rapid progress of PET imaging. One of these tracers, 2-deoxy-2-[^{18}F]fluoro-D-glucose ([^{18}F]FDG), is very widely used in tumor diagnosis, staging, and monitoring therapeutic response. Currently, the majority (~95%) of clinical PET scans use [^{18}F]FDG (1).

The molecular targets for [^{18}F]FDG are glucose transporters (e.g., GLUT1), and hexokinase. [^{18}F]FDG can first be recognized and transported into the cells by glucose transporters which are located on the cell membrane, and it is then phosphorylated by hexokinase to form 2-deoxy-2-[^{18}F]fluoro-D-glucose-6-phosphate ([^{18}F]FDG-6-phosphate). Because [^{18}F]FDG lacks a hydroxyl group in the 2-position, [^{18}F]FDG-6-phosphate cannot be further metabolized and this polar compound is metabolically trapped inside the cells (3, 4). The rationale for using [^{18}F]FDG as a general tumor marker relies on the fact that tumor cells often exhibit an increased glucose metabolism and an up-regulation of GLUT and hexokinase compared to non-neoplastic cells (5). The preferential accumulation of [^{18}F]FDG metabolites inside tumor cells compared to that in surrounding normal tissues makes the detection of tumors using PET possible. [^{18}F]FDG not only can be used in diagnosis and staging of cancer, but also is a powerful tool for monitoring disease recurrence and therapeutic efficacy (6–8). A recent excellent example of the latter is the use of [^{18}F]FDG-PET for monitoring treatment effects of imatinib mesylate (STI-571) on gastro-intestinal stromal tumors (9–10). The success of [^{18}F]FDG-PET for metabolic imaging of disease prompt scientist to develop glucose analogs labeled with less costly or therapeutic isotopes such as ^{99m}Tc and $^{186/188}$Re (11–12). Recently, it was reported that ^{99m}Tc labeled ethylenedicysteine–deoxyglucose (ECDG) can potentially be used for tumor imaging (11). However, further investigations are required to reveal the mechanism responsible for the accumulation of this probe in tumors, as well as to identify the specific molecular targets interacting with ^{99m}Tc-ECDG.

Although radionuclide imaging has several advantages including intrinsically high sensitivity, capability of quantitation and clinical translation, it often suffers from relatively low spatial resolution, high cost and limited radiation to personnel. Moreover, PET imaging often requires an on-site cyclotron and a radiochemistry laboratory to produce short half-life radionuclides and radiolabeled agents. Therefore, optical imaging (bioluminescence and fluorescence imaging) has emerged as an attractive imaging modality to study the biological/molecular events both in cell culture and in small living subjects. Optical imaging does not involve any ionizing radiation, it is inexpensive, highly sensitive and allows a high throughput screening since the acquisition times for obtaining a good image using optical imaging can be as short as seconds (13–14). Because of the strong tissue penetration ability of light in the near-infrared (NIR) region (650–900 nm wavelengths), near-infrared fluorescence (NIRF) imaging has emerged as a powerful tool for small animal imaging. Many studies have demonstrated that it is a viable method to noninvasively monitor disease states at the molecular level, localize cancer, and even assess the anti-tumor efficacy of new therapeutic drugs (15–18).

Considering the extensive applications of [^{18}F]FDG in nuclear medicine and rapid advancement in optical imaging, development of NIRF deoxyglucose analogs may serve as novel probes with the ability to evaluate the glucose metabolic rate of tumors. These probes could be useful for (a) accurate detection of abnormalities such as tumor and (b) noninvasive monitoring the therapeutic efficacy of drugs in living small animals. It was reported that a fluorescent derivative of 2-deoxyglucose, 2-[*N*-(7-nitrobenz-2-oxa-1,3-diazol-4-yl)amino]-2-deoxy-D-glucose (2-NBDG) (Ex: 475 nm; Em: 550 nm) can be delivered and trapped in cells via the GLUT/hexokinase pathway. Several studies demonstrated that the uptake of 2-NBDG (structure is shown in the Figure 1) can be inhibited by D-glucose, but not by L-glucose in different organisms (19–23). 2-NBDG can then be further metabolized to 2-NBDG-6-phosphate in *E. Coli* cells which was confirmed by mass spectrometry (21). These results highlight the possibility of preserving the GLUT/hexokinase targeting ability of the glucose analogs when they are conjugated with a bulk NIR fluorescent group at position 2 of deoxyglucose. A pyropheophorbide derivative of 2-deoxyglucose, Pyro-2DG, (Ex: 667 nm; Em: 679 and 720 nm, structure is shown in the Figure 1) was synthesized and also proved to be useful both as a tumor-targeted NIRF imaging probe and as a photodynamic therapy agent for treatment of tumor. Preliminary confocal fluorescence microscopy studies further shows that the uptake of Pyro-2DG in 9L glioma cells can be inhibited by 50 mM D-glucose, suggesting that Pyro-2DG is a substrate of GLUTs (24). Another interesting report tethered multiple D-(+)-glucosamines with cypate, a NIR chromophore core, to generate multivalent carbocyanine molecular beacons (structure of mono-D-(+)-glucosamine-containing cypate is shown in the Figure 1). Biodistribution studies in tumor bearing mice show that all the NIR fluorescent glucosamine derivatives localized in the tumor. But it is not clear whether their uptake and trapping in the tumor is through the GLUT/hexokinase pathway (25–26).

In this study, we first investigated the tumor cell uptake of 2-NBDG and the specificity of 2-NBDG toward GLUTs. We found that 2-NBDG is delivered and trapped in tumors cells via the GLUT, which is consistent with the recent report (27). The NIR fluorescent dye Cy5.5 has been proven to be a very useful fluorochrome for labeling biomolecules for in vivo optical imaging by several groups (28–35). Encouraged by the specific tumor cell uptake of 2-NBDG, we conjugated Cy5.5 monofunctional N-hydroxysuccinimide (NHS) ester (Cy5.5-NHS) and D-glucosamine to prepare a Cy5.5-D-glucosamine conjugate (Cy5.5-2DG) (see their structure in the Figure 1), and tested its feasibility for NIRF imaging of tumor in pre-clinical xenograft tumor models. As comparison, Cy5.5-NHS was also tested for its tumor targeting ability in vitro and in vivo. Furthermore, [^{18}F]FDG as a radioactive probe was utilized to image mice bearing U87MG tumors with microPET. We demonstrate the tumor specificity and long-lasting tumor accumulation of both fluorescent agents in human primary tumor cells in mouse xenografts.

EXPERIMENTAL PROCEDURES

Materials and General Methods

Cy5.5-NHS was purchased from Amersham Biosciences (Piscataway, NJ). All other reagents were obtained from Sigma-Aldrich Chemical Co. (St. Louis, MO). Matrix assisted laser desorption/ionization time of flight mass spectrometry (MALDI-TOF-MS) was performed by Stanford Protein and Nucleic Acid Biotechnology Facility, Stanford University. A Dionex Summit high-performance liquid chromatography (HPLC) system (Dionex Corporation, Sunnyvale, CA) equipped with a 170U 4-Channel UV-Vis absorbance detector was used for purification and analysis of Cy5.5 labeled compound. UV detection wavelengths were 218 nm, 280 nm and 590 nm for all the experiments. Both semipreparative (Zorbax SB-C18, 9.4 mm × 250 mm) and analytical (Dionex Acclaim 120 C18, 4.6 mm × 250 mm) reversed phase HPLC columns were used. The mobile phase was

solvent A, 0.1% trifluoroacetic acid (TFA) in water and solvent B, 0.1%TFA in acetonitrile (CH_3CN).

Synthesis and Characterization of Cy5.5-2DG

D-Glucosamine (30.2 mg) was dissolved in 302 μL H_2O to make a concentration of 463.7 mM solution. D-Glucosamine (34.5 μL, 16.0 μmol), sodium phosphate buffer (Na_2HPO_4, pH = 9.0, 0.1 M, 805.5 μL) and Cy5.5-NHS (1.81 mg, 1.60 μmol) dissolved in 160 μL H_2O were then mixed together. After overnight incubation at 4 °C in the dark, the reaction was quenched by adding 100 μL of 1% TFA. The crude product was then injected onto a semi-preparative HPLC column [the flow rate was 3.0 mL/min, with the mobile phase starting from 5% solvent B (0.1%TFA in CH_3CN) and 95% solvent A (0.1%TFA in water) (0–3 min) to 65% solvent B and 35% solvent A at 33 min, then going to 85% solvent B and 15% solvent A (33–36 min), maintaining this solvent composition for another three minutes (36–39 min) and returning to initial solvent composition by 42 min]. Fractions containing Cy5.5-2DG conjugate (retention time is 14.3 min) were collected, lyophilized, and identified by MALDI-TOF-MS. The chemical purity of product was determined by analytical HPLC (same gradient as used for semi-preparative HPLC; flow rate: 1.0 ml/min). The product was re-dissolved in saline at a concentration of 1 mg/mL, and stored in the dark at −80 °C until use. The absorbance spectrum of Cy5.5-2DG was rerecorded on an Agilent 8453 UV-visible ChemStation (Agilent Technologies, Wilmington, DE), and fluorescence spectrum of Cy5.5-2DG was measured on a Fluoromax-3 fluorophotometer (JOBIN YVON/ HORIBA, Edison, New Jersey).

Cell Lines and Tumor Xenografts

U87MG human glioblastoma cells, C6 rat glioma cells, A375M human melanoma cells, B16F10 murine melanoma cells and MDA-MB-435 human breast cancer cells were all obtained from American Type Culture Collection (Manassas, VA). U87MG, C6, A375M and B16F10 cells were cultured in Dulbecco's modified Eagle high glucose medium supplemented with 10% fetal bovine serum (FBS) and 1% penicillin-streptomycin (DMEM, Invitrogen Life Technologies, Carlsbad, CA). MDA-MB-435 was cultured in Leibovitz's L-15 medium with 2 mM L-glutamine supplemented with 0.01 mg/mL insulin, 10% FBS and 1% penicillin-streptomycin (Invitrogen Life Technologies, Carlsbad, CA). All the cell lines were maintained in a humidified atmosphere of 5% CO_2 at 37°C, with the medium changed every other day. A confluent monolayer was detached with trypsin and dissociated into a single cell suspension for further cell culture.

Animal procedures were performed according to a protocol approved by the Stanford University Administrative Panels on Laboratory Animal Care (A-PLAC). Female athymic nude mice (*nu/nu*), obtained from Charles River Laboratories, Inc. (Cambridge, MA) at 4–6 weeks of age, were subcutaneously injected in the right shoulder with 5×10^6 U87MG glioblastoma cells suspended in 100 μL of phosphate buffered saline (PBS, 0.01 mol/L; pH, 7.4). When the tumors reached 0.4–0.6 cm in diameter (14–21 days after implantation), the tumor bearing mice were subjected to in vivo imaging studies. In addition, 6 weeks old Fox chase ICR scid (severe combined immunodeficient) mice were inoculated with 4×10^6 A375M human melanoma cells. Three weeks to four weeks post-inoculation, the mice bearing A375M tumors were ready for further studies.

Fluorescence Microscopy and Cell Uptake Studies of 2-NBDG

For fluorescence microscopy studies, U87MG cells (1×10^5) were cultured on 35 mm MatTek glass bottom culture dishes (cat. no.: P35G-0-14-C, Ashland, MA). After 24 hours, the cells were washed with PBS and then incubated at 37 °C in the presence of 10 μM 2-NBDG for 10 minutes. After the incubation period, cells were washed three times with ice-

cold PBS. The fluorescence signal of the cells was recorded using an Axiovert 200M fluorescence microscope (Carl Zeiss MicroImaging, Inc., Thornwood, NY) equipped with a GFP filter set (Exciter, HQ 475/20 nm; Emitter, HQ 540/30 nm). An AttoArc HBO 100W microscopic illuminator was used as a light source for fluorescence excitation. Images were taken using a thermoelectrically cooled charged-coupled device (CCD) (Micromax, model RTE/CCD-576, Princeton Instruments Inc., Trenton, NJ) and analyzed using MetaMorph Software version 6.2r4 (Molecular Devices Corporation, Downingtown, PA). The effect of D-glucose or L-glucose on 2-NBDG accumulation in U87MG cells was also examined. In these studies, cells were pre-incubated with medium containing either 50 mM D-glucose or L-glucose for 0.5 hour at 37 °C. Cells were then incubated with 10 μM 2-NBDG for 10 minutes at 37 °C. After incubation, U87MG cells were washed three times with ice-cold PBS and subjected to fluorescence microscopy imaging.

The inhibition effect of D- or L-glucose on 2-NBDG uptake in U87MG cells was also assessed by measurement the fluorescence intensity of cells lysate. Briefly, the cultured U87MG human glioblastoma cells were trypsinized, washed twice with PBS and suspended at 10×10^6 cells/mL in PBS. Cells (1.0×10^6) were pre-incubated with either 10 mM, 50 mM D-glucose or 50 mM L-glucose for 30 minutes, then incubated with 50 μM 2-NBDG for another hour at 37 °C. The cells were centrifuged (250 *g*) for 3 min and washed three times with cold PBS. Cell pellets were then lysed with 150 μL of cold spectral grade water, following by freezing in dry ice. The frozen cell solution was thawed and centrifuged at 12,000*g* for 5 min. The fluorescence intensity of 100 μL of cell lysate was measured on a Fluoromax-3 fluorophotometer.

Fluorescence Microscopy Studies of Cy5.5-2DG and Cy5.5-NHS

Fluorescence microscopy imaging was performed to study the uptake of Cy5.5-2DG and Cy5.5-NHS by several tumor cell lines such as U87MG, C6, A375M, B16F10 and MDA-MB-435, as well as to exam the effect of D-glucose or L-glucose on 2-NBDG accumulation in U87MG cells. The procedure described in the above section was followed in this experiment, except that 100 nM Cy5.5-2DG or Cy5.5-NHS was used for incubation with cells and a Cy5.5 filter set was used in fluorescence microscope for the collection of the fluorescence signal.

Optical Imaging of Tumors in Mice

In vivo fluorescence imaging was performed with an IVIS 200 small animal imaging system (Xenogen, Alameda, CA). A Cy5.5 filter set was used for acquiring Cy5.5-2DG and Cy5.5-NHS fluorescence in vivo. Identical illumination settings (lamp voltage, filters, f/stop, field of views, binning) were used for acquiring all images, and fluorescence emission was normalized to photons per second per centimeter square per steradian ($p/s/cm^2/sr$). Images were acquired and analyzed using Living Image 2.5 software (Xenogen, Alameda, CA). Mice bearing either U87MG or A375M (n = 3 for each imaging probe) were injected via tail vein with 0.5 nmol Cy5.5-2DG or Cy5.5-NHS and subjected to optical imaging at various time points postinjection (pi). For scid mouse bearing A375M tumor, the fur covered the tumor and the right shoulder was shaved to reduce light absorbance and scattering. All NIR fluorescent images were acquired using 1 second exposure time (f/stop = 4) and displayed in the same scale of fluorescent intensity.

Fluorescence Microscopy Imaging of Fresh Tissue Slides

Following optical imaging, the mice bearing U87MG were euthanized 24 hours pi of fluorescent probe. Tumors were dissected, placed in tissue holders, and then filled with Tissue-Tek® Optimal Cutting Temperature Compound (Sakura Finetek USA, Inc. Torrance, CA) and immediately frozen in dry ice. They were sectioned into 200 μm transverse slices

using a tissue slicer. Fluorescence microscopy imaging of fresh tissue slides was then performed to determine the localization and distribution of the probe in the tumor. The images were taken with a 10× objective.

MicroPET Imaging of U87MG Tumor

PET imaging of tumor-bearing mice was performed on a microPET R4 rodent model scanner (Concorde Microsystems Inc, Knoxville, TN). The mice bearing U87MG glioblastoma were injected with 5.55 MBq (150 μCi) of [^{18}F]FDG. At 30, 60 and 120 min pi, the mice were anesthetized with 2% isoflurane, and placed in the prone position and near the center of the filed of view of a microPET scanner (Siemens Inc.). The 5-min static scans were obtained and the images were reconstructed by a two-dimensional ordered subsets expectation maximum (OSEM) algorithm. Regions of interest (ROIs) were then drawn over the tumor on decay-corrected whole-body coronal images. The counts per pixel per minute were obtained from the ROI and converted to counts per milliliter per minute by using a calibration constant. By assuming a tissue density of 1 g/mL, the ROI values were converted to counts/g/min. An image ROI-derived percentage ID per gram of tissue (%ID/g) was then determined by dividing counts per gram per minute with injected dose (ID).

Data Processing and Statistics

All the data are given as mean ± SD of *n* independent measurements. Statistical analysis was performed using a Student's *t*-test. Statistical significance was assigned for P values < 0.05. For determining tumor contrast, maximum fluorescence intensities (p/s/cm^2/sr) of the tumor area at the right shoulder of the animal (*T*) and of the area at the right flank [normal tissue (*N*)] were calculated by the region-of-interest (ROI) function of Living Image software integrated with Igor (Wavemetrics, Lake Oswego, OR). Dividing *T* by *N* yielded the contrast between tumor tissue and normal tissue.

RESULTS AND DISCUSSION

NIRF imaging is emerging as a powerful tool for noninvasive imaging diseases in pre-clinical models. It also has a great potential for clinical use in providing both real time surgical information and functional/molecular information of the disease. NIRF probes with capability of imaging specific molecular targets and events are therefore under active investigation. Our research was intended to develop NIR fluorescent glucose analogs for imaging tumor metabolism in living subjects. Although several NIR 2-deoxyglucose analogs which are able to accumulate in the tumors were successfully synthesized recently (24–26), whether these compounds are delivered and trapped in tumor cells via the GLUTs/hexokinase pathway remains to be answered. Moreover, the ability of these NIR 2-deoxyglucose analogs to imaging tumor metabolism in small animals has not been demonstrated yet.

It was reported that 2-NBDG could be incorporated by glucose transporting systems in living cells. More recently, it was found that 2-NBDG can accumulate into malignant tumor cells such as the MCF-7 breast cancer cells and the HepG2 liver cancer cells (27). In this work, the cell uptake of 2-NBDG by U87MG was also examined using fluorescence microscopy imaging. It was found 2-NBDG did accumulate in the cytoplasm of U87MG cells (Figure 2A–a, d). We also found this fluorescent glucose analog showed good uptake in several other tumor cell lines such as C6, A375M, B16F0, and MDA-MB-435 (data not shown). More importantly, uptake of 2-NBDG by U87MG was significantly inhibited by 10 mM and 50 mM D-glucose (P < 0.05) but not by 50 mM L-glucose (Figure 2A and 2B), strongly indicating that the uptake of 2-NBDG is likely mediated by glucose transporters.

However, the short excitation and emission wavelength (Ex: 475 nm; Em: 550 nm) of 2-NBDG limits its applications for imaging small living subjects.

Encouraged by these results, we hypothesized that conjugation of D-glucosamine with a carefully designed NIRF dye may generate a fluorescence deoxyglucose analog which can be still recognized by GLUTs and hexokinase. Therefore, Cy5.5-2DG was synthesized and evaluated in both cell culture and mice, because of the longer excitation/emission wavelengths of Cy5.5 and its easy availability. Synthesis of Cy5.5-2DG was achieved through conjugation of Cy5.5-NHS ester with the 2-amino group of the D-glucosamine. The desired products were purified by semi-preparative HPLC. The retention time on analytical HPLC for Cy5.5-2DG was found to be 15.2 minutes. The yield of Cy5.5-2DG conjugate was typically over 70%. The purity of Cy5.5-2DG was over 95% from analytical HPLC analysis. The purified Cy5.5-2DG was characterized by MALDI-TOF-MS. Cy5.5-2DG: *m/z* = 1078.26 for $[M+H]^+$ ($C_{47}H_{56}N_3O_{18}S_4$, calculated MW = 1078.24). The absorption and fluorescence emission characteristics of Cy5.5-2DG (λ_{ab} = 675 nm, λ_{em} = 695 nm) were identical to those of free Cy5.5, as apparent from the spectra measured in H_2O (Figure 3). The stability of Cy5.5-2DG was further evaluated by incubation the compound with mouse serum for 1 hour. No dissociation of Cy5.5 from Cy5.5-2DG conjugate was found by using HPLC analysis, suggesting the good serum stability of Cy5.5-2DG.

Fluorescence microscopy imaging studies were performed to investigate the cell uptake of Cy5.5-2DG in different tumor cell lines. It was found that Cy5.5-2DG does accumulate in several tumor cell lines such as A375M, B16F10, C6, U87MG, and MDA-MB-435 at 37 °C, while the uptake at 4 °C was minimal. This result indicates that the cellular uptake of Cy5.5-2DG is due to an active and temperature dependent process, instead of simple passive diffusion. In order to further elucidate whether its cell uptake is related to GLUTs, Cy5.5-2DG was incubated with either 50 mM D-glucose or L-glucose. However, Cy5.5-2DG localizes within U87MG cells with similar fluorescence intensity in the presence and absence of 50 mM D-glucose and L-glucose. D-Glucose failed to block the cell uptake of Cy5.5-2DG, suggesting GLUTs are not likely the transporter system responsible for Cy5.5-2DG uptake. In order to determine whether Cy5.5-2DG is a substrate for hexokinase, Cy5.5-2DG was incubated with glucose reagent (Infinity Glucose Reagent; ThermoDMA, Louisville, CO) at 37 °C for 3 minutes (12). From MALDI-TOF-MS analysis, we were not able to observe the formation of phosphorylated Cy5.5-2DG (data not shown). Cy5.5-2DG does not seem to mimic glucose/deoxyglucose phosphorylation. More studies are needed to pinpoint the uptake and retention mechanism of Cy5.5-2DG in cells.

For comparison, Cy5.5-NHS was used as a control for staining the tumor cell lines. Fluorescence microscopy imaging studies demonstrate that Cy5.5-NHS can label these tumor cell lines as well as Cy5.5-2DG at 37 °C, and also shows negligible fluorescence signal when incubated at 4 °C. In a previous study (28), it was reported that very little Cy5.5-NHS accumulates in two breast cancer cell lines, MDA-MB-648 and MDA-MB-435. This is likely due to different filter settings and detection sensitivity of the fluorescence microscopes used in our study compared to the published study. In that report, a 775 nm/845 nm (excitation/emission) filter was equipped to obtain Cy5.5 fluorescence images. However a Cy5.5 filter set (Exciter, 650/20 nm; Emitter, 675/35 nm) was used in our study. Considering the maximum excitation and emission wavelength of Cy5.5 dye is 675 nm and 694 nm respectively, the 775 nm/845 nm filter set is not the proper setting, and one is unlikely to observe enough Cy5.5 fluorescence signal using such a filter.

Whole-body optical imaging of subcutaneous tumor xenografted mice was then performed by using an IVIS200 system to monitor in vivo biodistribution of Cy5.5-2DG and Cy5.5-NHS. As shown in Figure 4A, the subcutaneous U87MG tumor could be clearly

distinguished from the surrounding background tissue from 30 min up to 24 h pi of either 0.5 nmol of Cy5.5-2DG or Cy5.5-NHS. Quantitative analysis of these images was performed, and the fluorescence intensities in the tumor and the normal tissues as a function of time for Cy5.5-2DG and Cy5.5-NHS are depicted in Figure 4B–C, respectively. It was found that both probes exhibited fast tumor targeting characteristics in vivo. The tumor uptake of Cy5.5-2DG and Cy5.5-NHS reached a maximum 30 minutes pi and slowly washed out over time. A similar pattern was found for the uptake of both probes in normal tissue. At all time points pi (0.5 h to 24 h), there is no statistical significant difference in tumor and normal tissue uptake between Cy5.5-2DG and Cy5.5-NHS ($P > 0.05$) (Figure 4B–C). The fluorescence intensity ratio between the tumor and normal tissue (*T/N*) for Cy5.5-2DG (represented by solid line) and Cy5.5-NHS (represented by dotted line) was calculated and shown in Figure 4D. Cy5.5-NHS shows significantly higher *T/N* ratio than Cy5.5-2DG at later time points (4 h and 24 h) ($P < 0.05$). For example, *T/N* ratio for Cy5.5-2DG, and Cy5.5-NHS are found to be 2.81 ± 0.10 and 3.34 ± 0.23, respectively, at 24 h pi. U87MG tumor tissues from the mice 24 h after administration of fluorescent probes were then taken out and sliced for NIRF imaging. Fluorescence and brightfield images for the tumor slices of mice injected with Cy5.5-2DG and Cy5.5-NHS were obtained. It was found that both probes accumulate in the tumor cells, and the fluorescence intensity is similar in both samples.

The tumor targeting abilities in living subjects of Cy5.5-2DG and Cy5.5-NHS were also evaluated in A375M xenografted mouse model. Figure 5A shows typical NIR fluorescence images of scid mice bearing subcutaneous A375M melanoma tumor after intravenous (iv) injection of 0.5 nmol of probe. Similar as the distribution in U87MG mouse, both Cy5.5-2DG and Cy5.5-NHS show higher uptake in the tumor compared to normal tissue uptake. Moreover, significant difference in *T/N* is observed between Cy5.5-2DG and Cy5.5-NHS at 48 hours pi ($P = 0.01$). The *T/N* ratio for Cy5.5-2DG, Cy5.5-NHS at 48 hours are 1.63 ± 0.06 and 2.58 ± 0.36, respectively (Figure 5B).

The radioactive DEOXYGLUCOSE analog, [^{18}F]FDG was then used to image the nude mice bearing human U87MG using microPET. [^{18}F]FDG preferentially localizes and is retained in U87MG tumors, as clearly shown in Figure 6A. The tumor/muscle ratios are 3.89 ± 0.99, 3.96 ± 0.39, and 4.08 ± 0.65, at 30 min, 1 h and 2 h pi of the probe. Obviously, the tumor contrast for [^{18}F]FDG at these time points is significantly higher than that of Cy5.5-2DG (*T/N* ratios at 30 min to 2 h pi are all below 2, as shown in Figure 4D). This is probably caused by: 1). conjugation D-glucose with a big fluorophor Cy5.5 resulting in a compound with reduced cell uptake and/or retention; 2) auto-fluorescence of normal tissue increasing the background signal. Furthermore, compared to optical imaging, [^{18}F]FDG-microPET is able to quantify the probe accumulation in most organs of interest such as brain, heart, kidney, etc. However, except for the disadvantages as described in the introduction, PET imaging can only monitor the [^{18}F]FDG distribution up to several half lives of F-18. While optical imaging can observe the Cy5.5-2DG NIR signal in living mouse even several days pi.

The small animal optical imaging data shows that both Cy5.5-2DG and Cy5.5-NHS can accumulate very well in U87MG and A375M tumor models. Even 4 days pi of the probes, the tumor showed the high fluorescent signal and could be clearly visualized (data not shown). Another preliminary study also revealed that Cy5.5-2DG and Cy5.5-NHS can localize in the MDA-MB-435 tumor in an orthotopic tumor model (data not shown). Although it is not clear how Cy5.5-2DG and Cy5.5-NHS localize and are retained in the tumor, their high specificity, high accumulation and retention in tumors will likely make them very useful in 1) labeling cancer cells for cell trafficking; 2) in vivo staining of tumor such as breast cancer, melanoma, and glioma for guidance of tumor surgery and radiation therapy in conjunction with proper optical imaging systems, etc. Moreover, conjugation of

Cy5.5-NHS with cancer chemotherapeutical drugs or radionuclides such as F-18 may generate novel tumor targeting agents.

The in vivo tumor seeking ability of Cy5.5-NHS documented here is very different from the results reported previously (28). In that report, the authors did not observe any significant difference between the uptake in the tumor region and normal tissue region after injection of Cy5.5-NHS. This inconsistency may be due to several factors such as the depth and size of tumor, different settings of the optical imaging system, and the amount of dye injected (2.9 nmol/mouse in their report vs 0.5 nmol/mouse in our study), etc. Our finding also highlight the importance of a complete separation of free Cy5.5-NHS and Cy5.5 labeled biomolecules (peptides or antibodies, etc) in order to avoid any false-positive results.

Based on our data reported here and previous reports (19–23), 2-NBDG has been proven to be a substrate of GLUTs, while Cy5.5-2DG is not. Considering Cy5.5 is a much larger molecule than 2-[*N*-(7-nitrobenz-2-oxa-1,3-diazol-4-yl)amino] (NBD) moiety (Figure 1), it is likely that size of the fluorophor in the 2 position is the reason that Cy5.5-2DG cannot be delivered and trapped in tumor cells via the GLUT/hexokinase pathway. It looks like the resulting conjugate no longer behaves like D-glucose if the dye gets too large. These results clearly suggest the importance of selection of NIR dyes for preparation of NIRF D-glucose analogs.

In conclusion, the NIRF glucose analog, Cy5.5-DG and Cy5.5-NHS both demonstrate tumor targeting abilities in cell culture and in living mice but not through the GLUT/hexokinase pathway. More studies are warranted to further explore these two imaging probes for optical tumor imaging in cell culture and living subjects.

Abbreviatons

NIRF	near-infrared fluorescence
Cy5.5-2DG	Cy5.5-D-glucosamine
[^{18}F]FDG	2-deoxy-2-[^{18}F]fluoro-D-glucose
HPLC	high-performance liquid chromatography
PET	positron emission tomography
pi	postinjection

Acknowledgments

We thank Dr. Bengang Xing for technical assistance on fluorescent microscopy imaging. This work was supported, in part, by National Cancer Institute (NCI) Small Animal Imaging Resource Program (SAIRP) grant R24 CA93862, and NCI In Vivo Cellular Molecular Imaging Center (ICMIC) grant P50 CA114747 (SSG).

LITERATURE CITED

1. Gambhir SS. Molecular imaging of cancer with positron emission tomography. Nat. Rev. Cancer. 2002; 2:683–693. [PubMed: 12209157]
2. Nabi HA, Zubeldia JM. Clinical applications of ^{18}F-FDG in oncology. J. Nucl. Med. Technol. 2002; 30:3–9. [PubMed: 11948260]
3. Wahl, R. Positron emission tomography: applications in oncology. In: Henkin, RV.; Boles, MA.; Dillehay, GL., et al., editors. Nuclear Medicine. St. Louis, MO: Mosby; 1996. p. 1524-1545.
4. Kaarstad K, Bender D, Bentzen L, Munk OL, Keiding S. Metabolic fate of ^{18}F-FDG in mice bearing either SCCVII squamous cell carcinoma or C3H mammary carcinoma. J. Nucl. Med. 2002; 43:940–947. [PubMed: 12097467]

5. Warburg, O. The Metabolism of Tumors. New York, NY: Richard R. Smith, Inc; 1931. p. 129-169.
6. Wahl RL, Zasadny K, Helvie M, Hutchins GD, Weber B, Cody R. Metabolic monitoring of breast cancer chemohormonotherapy using positron emission tomography: initial evaluation. J. Clin. Oncol. 1993; 11:2101–2111. [PubMed: 8229124]
7. Lapela M, Eigtved A, Jyrkkio S, Grenman R, Kurki T, Lindholm P, Nuutinen J, Sutinen E, Solin O, Bjornskov I, Bretlau P, Friberg L, Holm S, Jensen M, Sand Hansen H, Minn H. Experience in qualitative and quantitative FDG PET in follow-up of patients with suspected recurrence from head and neck cancer. Eur. J. Cancer. 2000; 36:858–867. [PubMed: 10785590]
8. Akhurst T, Downey RJ, Ginsberg MS, Gonen M, Bains M, Korst R, Ginsberg RJ, Rusch VW, Larson SM. An initial experience with FDG-PET in the imaging of residual disease after induction therapy for lung cancer. Ann. Thoracic Surg. 2002; 73:259–264.
9. Gayed I, Vu T, Iyer R, Johnson M, Macapinlac H, Swanston N, Podoloff D. The role of ^{18}F-FDG PET in staging and early prediction of response to therapy of recurrent gastrointestinal stromal tumors. J. Nucl. Med. 2004; 45:17–21. [PubMed: 14734662]
10. Joensuu H, Roberts PJ, Sarlomo-Rikala M, Andersson LC, Tervahartiala P, Tuveson D, Silberman S, Capdeville R, Dimitrijevic S, Druker B, Demetri GD. Effect of the tyrosine kinase inhibitor STI571 in a patient with a metastatic gastrointestinal stromal tumor. N. Engl. J. Med. 2001; 344:1052–1056. [PubMed: 11287975]
11. Schibli R, Dumas C, Petrig J, Spadola L, Scapozza L, Garcia-Garayoa E, Schubiger PA. Synthesis and in vitro characterization of organometallic rhenium and technetium glucose complexes against Glut 1 and hexokinase. Bioconjugate Chem. 2005; 16:105–112.
12. Yang DJ, Kim CG, Schechter NR, Azhdarinia A, Yu DF, Oh CS, Bryant JL, Won JJ, Kim EE, Podoloff DA. Imaging with ^{99m}Tc ECDG targeted at the multifunctional glucose transport system: feasibility study with rodents. Radiology. 2003; 226:465–473. [PubMed: 12563141]
13. Massoud TF, Gambhir SS. Molecular imaging in living subjects: seeing fundamental biological processes in a new light. Genes Dev. 2003; 17:545–580. [PubMed: 12629038]
14. Ntziachristos V, Bremer C, Weissleder R. Fluorescence imaging with near-infrared light: new technological advances that enable in vivo molecular imaging. Eur. Radiol. 2003; 13:195–208. [PubMed: 12541130]
15. Mahmood U, Weissleder R. Near-infrared optical imaging of proteases in cancer. Mol. Cancer Ther. 2003; 2:489–496. [PubMed: 12748311]
16. Achilefu S. Lighting up tumors with receptor-specific optical molecular probes. Technol. Cancer Res. Treat. 2004; 3:393–409. [PubMed: 15270591]
17. Sevick-Muraca EM, Houston JP, Gurfinkel M. Fluorescence-enhanced, near-infrared diagnostic imaging with contrast agents. Curr. Opin. Chem. Biol. 2002; 6:642–650. [PubMed: 12413549]
18. Hawrysz DJ, Sevick-Muraca EM. Developments toward diagnostic breast cancer imaging using near-infrared optical measurements and fluorescent contrast agents. Neoplasia. 2000; 2:388–417. [PubMed: 11191107]
19. Yamada K, Nakata M, Horimoto N, Saito M, Matsuoka H, Inagaki N. Measurement of glucose uptake and intracellular calcium concentration in single, living pancreatic beta-cells. J. Biol. Chem. 2000; 275:22278–22283. [PubMed: 10748091]
20. Yoshioka K, Takahashi H, Homma T, Saito M, Oh KB, Nemoto Y, Matsuoka H. A novel fluorescent derivative of glucose applicable to the assessment of glucose uptake activity of Escherichia coli. Biochim. Biophys. Acta. 1996; 1289:5–9. [PubMed: 8605231]
21. Yoshioka K, Saito M, Oh KB, Nemoto Y, Matsuoka H, Natsume M, Abe H. Intracellular fate of 2-NBDG, a fluorescent probe for glucose uptake activity, in Escherichia coli cells. Biosci. Biotechnol. Biochem. 1996; 60:1899–1901. [PubMed: 8987871]
22. Lloyd PG, Hardin CD, Sturek M. Examining glucose transport in single vascular smooth muscle cells with a fluorescent glucose analog. Physiol. Res. 1999; 48:401–410. [PubMed: 10783904]
23. Oh KB, Matsuoka H. Rapid viability assessment of yeast cells using vital staining with 2-NBDG, a fluorescent derivative of glucose. Int. J. Food Microbiol. 2002; 76:47–53. [PubMed: 12038577]
24. Zhang M, Zhang Z, Blessington D, Li H, Busch TM, Madrak V, Miles J, Chance B, Glickson JD, Zheng G. Pyropheophorbide 2-deoxyglucosamide: a new photosensitizer targeting glucose transporters. Bioconjugate Chem. 2003; 14:709–714.

25. Ye Y, Bloch S, Achilefu S. Polyvalent carbocyanine molecular beacons for molecular recognitions. J. Am. Chem. Soc. 2004; 126:7740–7741. [PubMed: 15212497]
26. Ye Y, Bloch S, Kao J, Achilefu S. Multivalent carbocyanine molecular probes: synthesis and applications. Bioconjugate Chem. 2005; 16:51–61.
27. O'Neil RG, Wu L, Mullani N. Uptake of a fluorescent deoxyglucose analog (2-NBDG) in tumor cells. Mol. Imaging Biol. 2005; 7:1–5.
28. Ke S, Wen X, Gurfinkel M, Charnsangavej C, Wallace S, Sevick-Muraca EM, Li C. Near-infrared optical imaging of epidermal growth factor receptor in breast cancer xenografts. Cancer Res. 2003; 63:7870–7875. [PubMed: 14633715]
29. Ballou B, Fisher GW, Deng JS, Hakala TR, Srivastava M, Farkas DL. Cyanine fluorochrome-labeled antibodies in vivo: assessment of tumor imaging using Cy3, Cy5, Cy5.5, and Cy7. Cancer Detect. Prev. 1998; 22:251–257. [PubMed: 9618048]
30. Chen X, Conti PS, Moats RA. In vivo near-infrared fluorescence imaging of integrin $\alpha_v\beta_3$ in brain tumor xenografts. Cancer Res. 2004; 64:8009–8014. [PubMed: 15520209]
31. Ntziachristos V, Schellenberger EA, Ripoll J, Yessayan D, Graves E, Bogdanov A Jr, Josephson L, Weissleder R. Visualization of antitumor treatment by means of fluorescence molecular tomography with an annexin V-Cy5.5 conjugate. Proc. Natl. Acad. Sci. U. S. A. 2004; 101:12294–12299. [PubMed: 15304657]
32. Law B, Curino A, Bugge TH, Weissleder R, Tung CH. Design, synthesis, and characterization of urokinase plasminogen-activator-sensitive near-infrared reporter. Chem. Biol. 2004; 11:99–106. [PubMed: 15112999]
33. Hansch A, Frey O, Hilger I, Sauner D, Haas M, Schmidt D, Kurrat C, Gajda M, Malich A, Brauer R, Kaiser WA. Diagnosis of arthritis using near-infrared fluorochrome Cy5.5. Invest Radiol. 2004; 39:626–632. [PubMed: 15377942]
34. Ballou B, Fisher GW, Waggoner AS, Farkas DL, Reiland JM, Jaffe R, Mujumdar RB, Mujumdar SR, Hakala TR. Tumor labeling in vivo using cyanine-conjugated monoclonal antibodies. Cancer Immunol. Immunother. 1995; 41:257–263. [PubMed: 7489569]
35. Cheng Z, Wu Y, Xiong ZM, Gambhir SS, Chen X. Near-Infrared fluorescent RGD peptides for optical imaging of integrin $\alpha_v\beta_3$ expression in living mice. Bioconjugate Chem. 2005; 16:1433–1441.

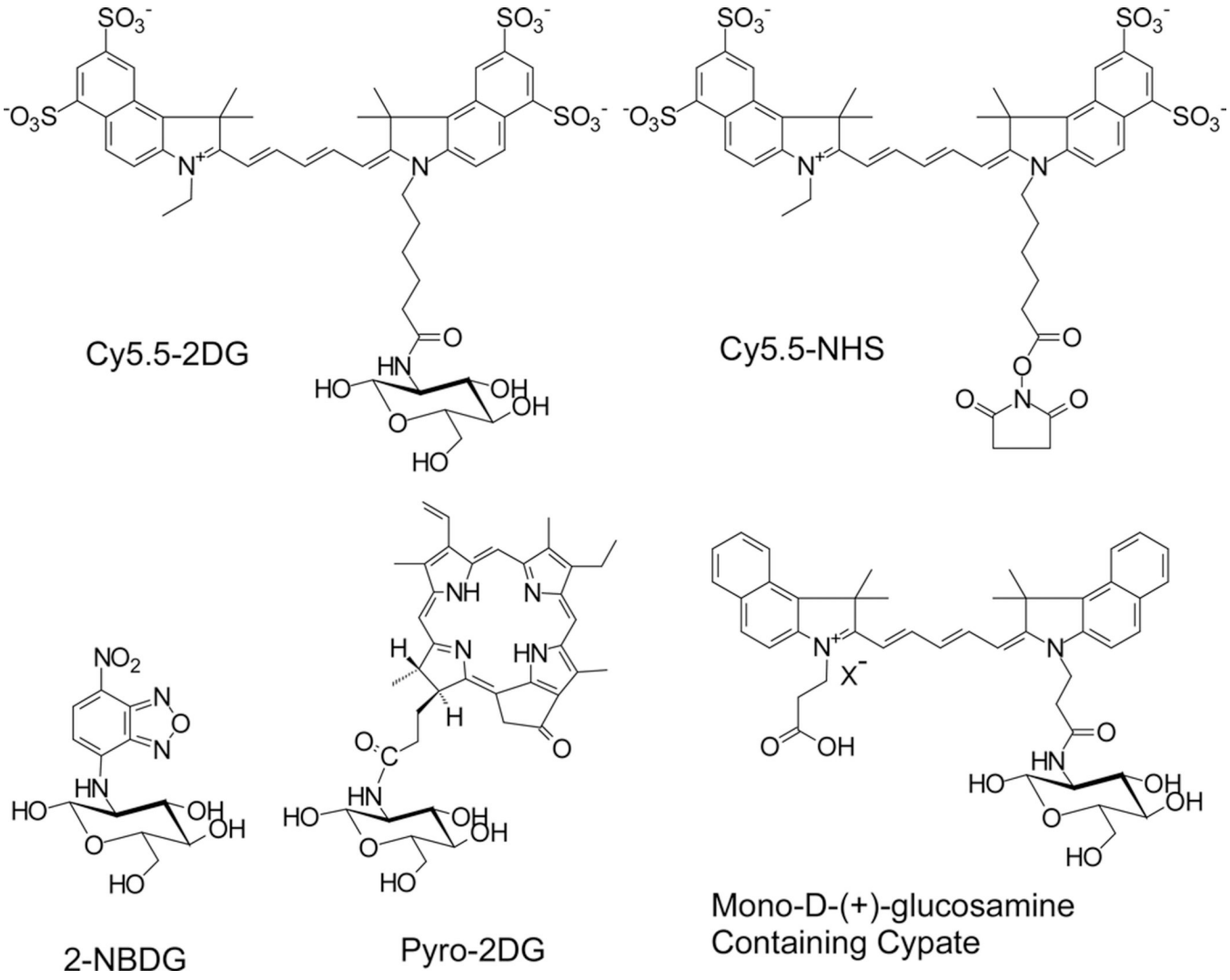

Figure 1.
Schematic structures of Cy5.5-2DG, Cy5.5-NHS, 2-NBDG, Py-2DG, and mono-D-(+)-glucosamine-containing cypate.

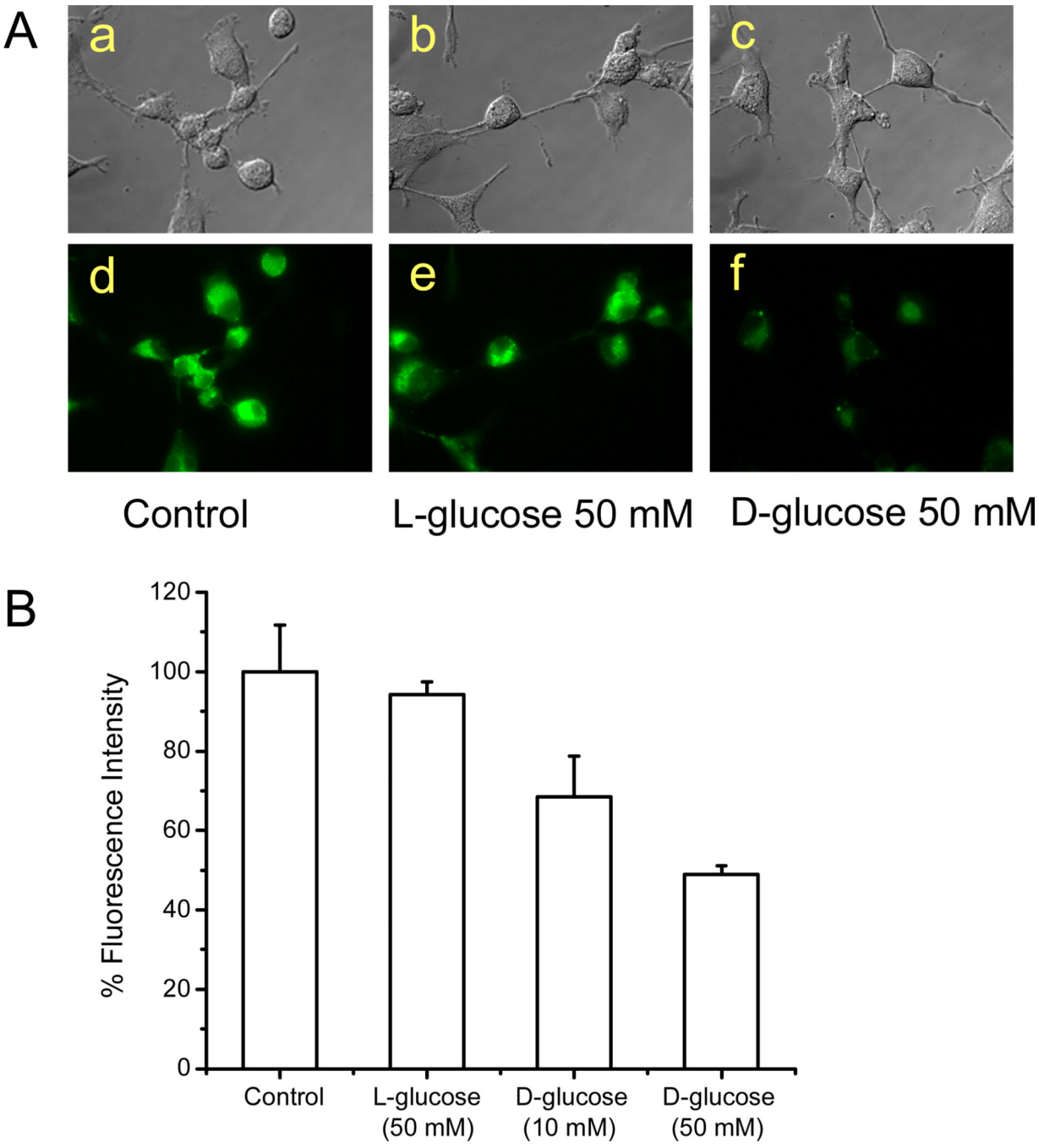

Figure 2.

(A) Light (top panel) and fluorescence (bottom panel) images of U87MG cells. The cells were incubated with 10 μM 2-NBDG for 10 min at 37 °C in the absence of D or L-glucose (a and b), and presence of 50 mM L-glucose (b and e) and 50 mM D-glucose. The images show the 2-NBDG accumulates in the cytoplasm of cells, and the 2-NBDG fluorescence in cells can be competitively inhibited by D-glucose but not by L-glucose. (B) Significant inhibition of the 2-NBDG uptake by U87MG cells by 10 mM and 50 mM D-glucose ($P < 0.05$), but not by 50 mM L-glucose, as measured by fluorescence intensity with a spectrofluorometer.

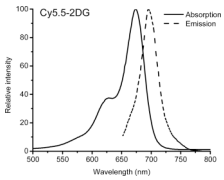

Figure 3.
Absorption (675 nm) and emission fluorescence (695 nm) spectra of Cy5.5-2DG in water.

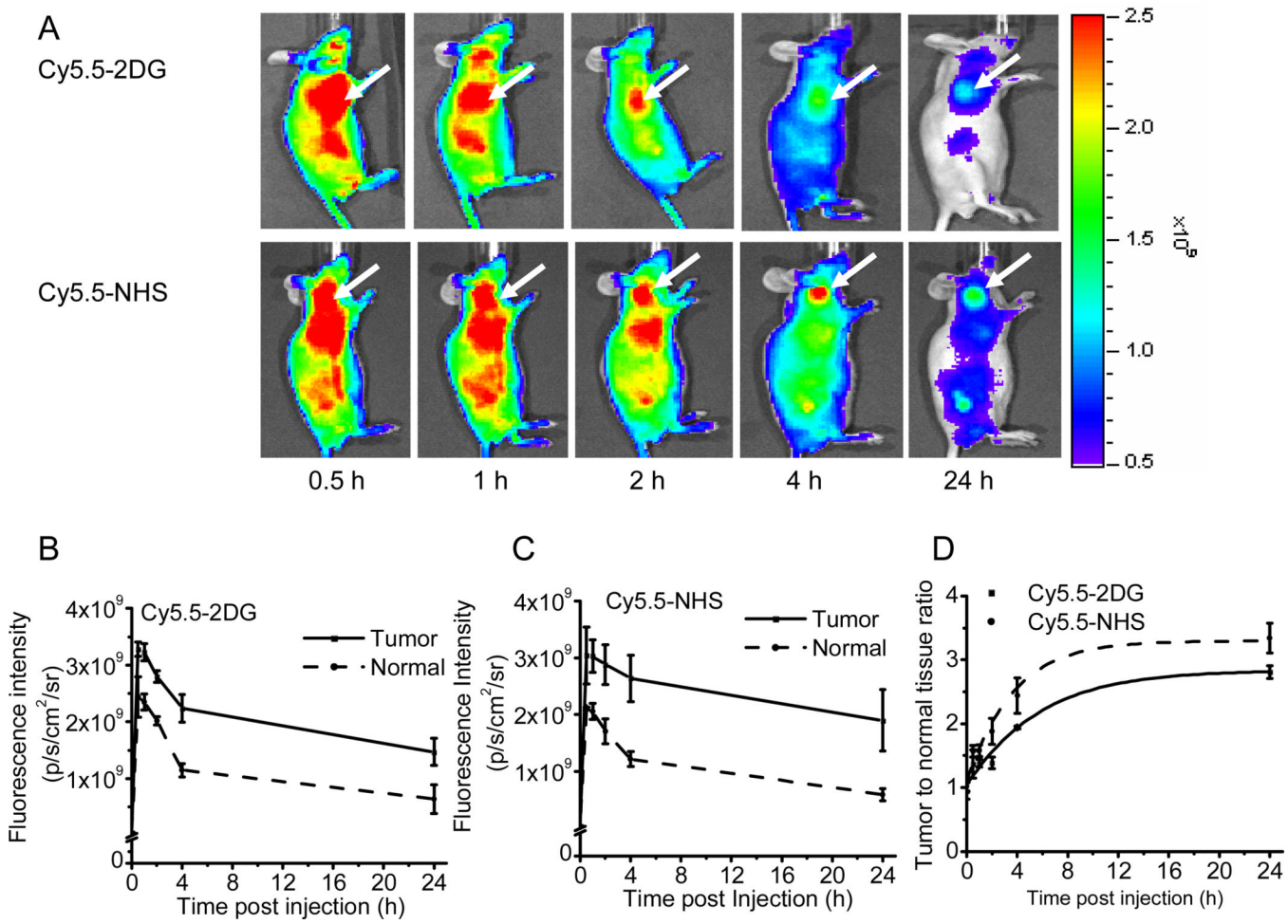

Figure 4.

(A) In vivo fluorescence imaging of subcutaneous U87MG glioblastoma tumor bearing nude mice after intravenous injection of 0.5 nmol Cy5.5-2DG (top) or Cy5.5-NHS (bottom). The position of the tumor is indicated by an arrow. Fluorescence signal from probes was pseudo-colored red. Quantification and kinetics of in vivo targeting charactereristics of Cy5.5-2DG (B) and Cy5.5-NHS (C). Fluorescence intensity was recorded as photons per second per centimeter square per steradian (*p/s/cm2/sr*). Tumor fluorescence was higher than that in the normal tissue. (D) Tumor contrast (tumor-to-normal tissue ratio) as a function of time post-administration of Cy5.5-2DG (■, solid line) and Cy5.5-NHS (◆, dotted line). The tumor to normal tissue ratio of Cy5.5-NHS at 4 h and 24 h post-injection is significantly higher than that of Cy5.5-2DG ($P < 0.05$).

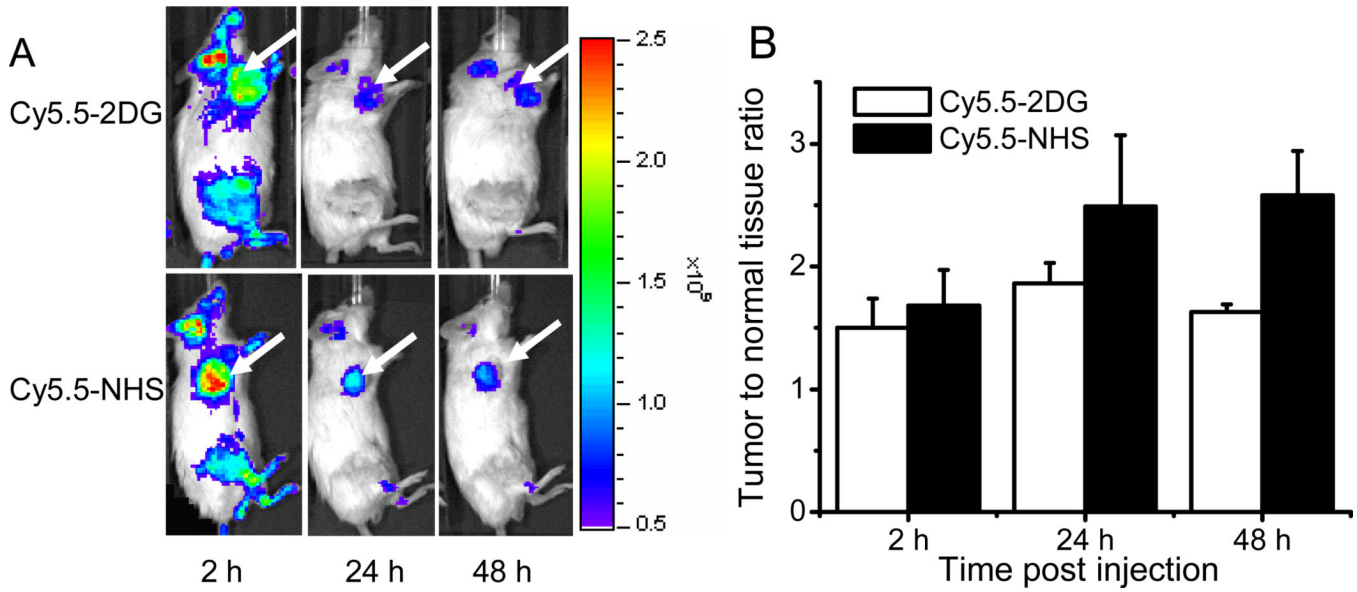

Figure 5.

(A) In vivo NIRF images of subcutaneous A375M melanoma bearing scid mice after intravenous injection of 0.5 nmol Cy5.5-2DG (top) and Cy5.5-NHS (bottom). The position of the A375M tumor is indicated by an arrow. Fluorescence signal from NIRF probes was pseudo-colored red. Tumor can be clearly visualized at 2 h up to 48 h pi (B) Tumor-to-normal tissue ratio at 2 h, 24 h and 48 h post-administration of Cy5.5-2DG (□) and Cy5.5-NHS (■). The tumor contrast of Cy5.5-NHS at 48 h post-injection is significantly higher than that of Cy5.5-2DG ($P < 0.05$).

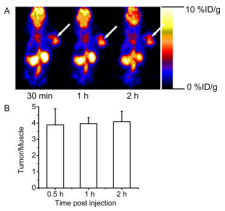

Figure 6.

(A) Decay-corrected whole-body coronal microPET images of nude mouse bearing human U87MG tumor at 30 min, 1 h, and 2 h (5-min static image) after injection of 5.55 MBq (150 μCi) of [^{18}F]FDG. The position of the U87MG tumor is indicated by an arrow. (B) Tumor-to-normal tissue ratio at 30 min, 1 h and 2 h post-injection of [^{18}F]FDG, uptake values for organs derived from a multiple time-point microPET study. ROIs are shown as the mean %ID/g ± SD (*n*= 3).